JCIM JOURNAL OF CHEMICAL INFORMATION AND MODELING

pubs.acs.org/jcim Article

Structure of POPC Lipid Bilayers in OPLS3e Force Field

Milla Kurki, Antti Poso, Piia Bartos,*,‡ and Markus S. Miettinen‡

Cite This: J. Chem. Inf. Model. 2022, 62, 6462−6474 Read Online

ACCESS | Metrics & More | Article Recommendations | Supporting Information

ABSTRACT: It is crucial for molecular dynamics simulations of biomembranes that the force field parameters give a realistic model of the membrane behavior. In this study, we examined the OPLS3e force field for the carbon−hydrogen order parameters S_{CH} of POPC (1-palmitoyl-2-oleoylphosphatidylcholine) lipid bilayers at varying hydration conditions and ion concentrations. The results show that OPLS3e behaves similarly to the CHARMM36 force field and relatively accurately follows the experimentally measured S_{CH} for the lipid headgroup, the glycerol backbone, and the acyl tails. Thus, OPLS3e is a good choice for POPC bilayer simulations under many biologically relevant conditions. The exception are systems with an abundancy of ions, as similarly to most other force fields OPLS3e strongly overestimates the membrane-binding of cations, especially Ca^{2+}. This leads to undesirable positive charge of the membrane surface and drastically lowers the concentration of Ca^{2+} in the surrounding solvent, which might cause issues in systems sensitive to correct charge distribution profiles across the membrane.

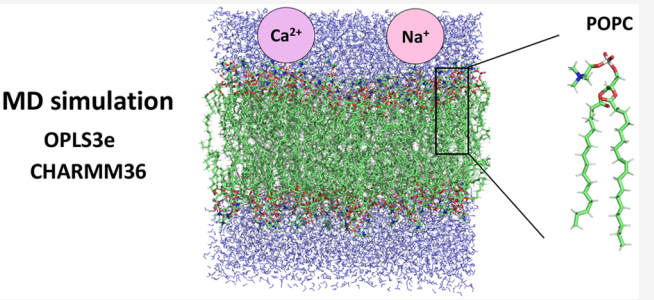

INTRODUCTION

Membranes function as biological barriers that separate cells from the environment and delineate different cellular compartments; they are crucial in maintaining the life-sustaining chemical and electrical gradients. The key structural constituents of membranes are phospholipids that form the membrane surface with their polar head groups and the membrane core with their lipophilic tails (Figure 1). In addition to phospholipids, biological membranes contain for example cholesterol, proteins, ions, and oligosaccharides. Lipid bilayers play central role in several biological and pathological processes such as cell division, intracellular membrane trafficking, and formation of lipid rafts.[1,2] To fully understand these processes, atomistic and molecular level understanding of lipids is required.[3] Such understanding can be obtained through computational tools, but it is important that those tools depict the structure, dynamics, and function of lipid bilayers accurately. Accurate lipid models allow the reliable study of, for example, membrane-bound proteins, transport through membranes, and pharmacokinetics of drugs.[4−6]

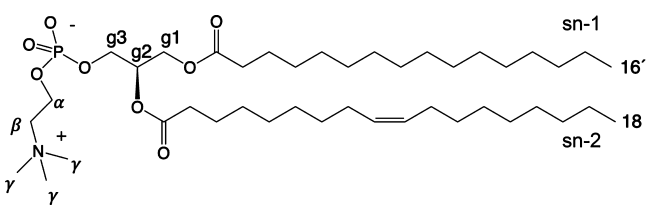

Figure 1. Chemical structure of 1-palmitoyl-2-oleoylphosphatidylcholine (POPC).

Why Accurate Force Field Parameters Are Important. Force field accuracy is of key importance in atomistic molecular dynamics (MD) simulation methods. Atomistic MD enables studying systems of interest in life sciences by a balance between computing power and precision: instead of the computationally heavy methods needed to describe quantum mechanical behavior, MD uses typically classical mechanics approximation (called force field) to reproduce molecular behavior. Thus, the validity of MD simulation studies relies heavily on the accuracy of the force field. Not surprisingly, a lot of effort has gone into force field development since the start of MD simulation studies in the 1980s.[7−11]

OPLS3e Force Field. OPLS3e is one of the most recent updates in the OPLS force field series available in the Schrödinger software suite.[12] OPLS3e has become widely used in drug discovery and material sciences due to its wide coverage of small molecules and accurate description of protein−ligand interactions. OPLS3e relies heavily on the earlier OPLS3 force field,[13] but with an addition and refinement of torsional parameters and a better handling of

Special Issue: Advancing Women in Chemistry

Received: April 6, 2022
Published: August 31, 2022

partial charges to offer improved accuracy on small-molecule conformational propensities, solvation, and protein−ligand binding. OPLS3e supports membrane simulations and offers optimized parameters for certain lipids: POPC (Figure 1), DMPC (1,2-dimyristoylphosphatidylcholine), DPPC (1,2-dipalmitoylphosphatidylcholine), and POPE (1-palmitoyl-2-oleoyl-phosphatidylethanolamine). Schrödinger has not, however, made publicly available the OPLS3e force field parameters or the procedure of lipid parameter validation; to our knowledge the accuracy of lipid simulations using OPLS3e, or its predecessor OPLS3, has also not been reported by others. To examine the performance of OPLS3e and to get an insight into how realistic model of lipid bilayers it produces, we simulated pure POPC bilayers at different conditions using the OPLS3e force field. We chose POPC among the OPLS3e-parametrized lipids due to its abundance in biological membranes and the availability of experimental data in the literature.

Performance of a force field can be assessed by comparing different observables between relevant experiments and MD simulations. For membrane lipids, the C−H bond order parameters S_{CH} offer an appealing option for such a task since they can be accurately measured experimentally using ^{2}H NMR[14] or ^{1}H−^{13}C NMR[15−17] techniques, and easily and directly calculated in MD simulations. The S_{CH} have a long history in force field validation for lipids and a large amount of experimental data are available in the literature.[3] Finally, as S_{CH} can be calculated for every C−H bond of the lipid molecule, they offer a very localized picture of the possible deficiencies of the simulation model.[3]

Lipids in Other Force Fields. Previous studies comparing experimental data to simulations show that in general, acyl chains of lipids are usually rather well described in simulations, and agreement of the structure and behavior of this region between the simulation and the experimental data is quite good.[3,18−20] However, correct description of headgroups and glycerol backbone has proven to be more challenging, and large variation in performance with different force fields occurs.[21−24] Predictive power of MD simulations on lipid structure usually decreases close to the water−lipid interfacial region, and more attention for the modeling of this region has been put in lately.[3,25−27]

Atomistic MD simulations of membrane systems have been previously used to research the effects of changing different physiologically relevant conditions, such as the hydration level and ion concentrations.[21,28−32] Lower hydration is relevant in studying many biological processes, such as membrane fusion;[33] ions are present in all biological systems, and ion−membrane interactions are of key importance, e.g., in neuron studies.[34−36] Experimental studies have shown that the phosphatidylcholine headgroup order parameters rise in response to lowering hydration and drop in response to cation binding.[3] A good-quality atomistic-level force field should also capture these changes.

Response to lowering hydration level is qualitatively correctly produced by several current force fields; but large variation occurs in description of cation binding, which is typically highly overestimated.[21,28,32,37,38] There are challenges in the correct description of Na^+ binding, but especially in the correct description of multivalent ions: Ca^{2+} overaccumulates at the membrane−water interface in most of the currently used force fields.[23,24,28]

CHARMM36 is one of the most used lipid force fields; and as it performs quite well in most lipid studies, we use it here as a reference.

In this study, we examined the performance of OPLS3e force field in membrane simulations. We demonstrate that OPLS3e produces C−H bond order parameters for POPC that are very close to experimental values and very similar when compared to the CHARMM36 force field. That said, in OPLS3e, as in many other force fields, the characterization of (especially of Ca^{2+}) ion binding to membrane seems problematic.

METHODS

Order Parameters. In this work the C−H bond order parameters S_{CH} are used to assess the force field performance. The S_{CH} depend on the angle θ between a C−H bond vector and the membrane normal (in our simulations the z-axis direction) as

$$S_{CH} = \frac{1}{2}\langle 3\cos^2\theta - 1\rangle \quad (1)$$

where the angular brackets denote average over the sampled conformations. Order parameters from simulations can be calculated directly from the atomic coordinates using the eq 1.

Experimental order parameters can be determined for lipid C−H bonds with NMR techniques, such as ^{2}H NMR[14] and ^{1}H−^{13}C NMR,[15−17] using quadrupolar splitting and dipolar splitting, respectively. These methods are very accurate and highly sensitive to changes in the lipid structural ensemble.[3] There are large amounts of experimental S_{CH} data available in the literature for different lipids measured with both ^{2}H and ^{13}C NMR, all in good agreement with each other.[21] Experimental order parameters have been estimated to have at least ±0.02 accuracy;[15,21] the error range of 0.02 is used also in this study, as suggested by Botan et al.,[21] as a sweet spot within which simulated order parameters should ideally reside compared to experimental data. Error range of 0.02 applies to magnitudes but relative changes in S_{CH} can be measured with much higher accuracy if the same equipment is used, allowing tracing of minor changes, such as the response to lowering hydration or additional salt;[21,28] this is utilized also in this study, for more discussion see ref 39.

Simulations. To compare the OPLS3e and CHARMM36 force fields to experimental data, we performed equally long MD simulations (lengths ranging from 500 ns to 1 μs) using both force fields with matching hydration levels (Table 1) and

Table 1. Simulated Lipid Bilayer Systems with Varying Hydration Levels[a]

force field	lipid	$N_{w/l}$	N_w	t_{sim} (ns)	t_{anal} (ns)	files
OPLS3e[12]	POPC	44	8859	500	500	43
	POPC	20	4000	500	490	44
	POPC	10	2000	500	495	45
	POPC	5	1000	1000	600	46
CHARMM36[47]	POPC	44	8880	500	460	48
	POPC	20	4000	500	400	49
	POPC	10	2000	500	425	50
	POPC	5	1000	1000	650	51

[a] $N_{w/l}$: Water/lipid ratio. N_w: Number of water molecules. t_{sim}: Total simulation time. t_{anal}: Time used for analysis. Files: Reference containing the simulation files.

https://doi.org/10.1021/acs.jcim.2c00395
J. Chem. Inf. Model. 2022, 62, 6462−6474

Table 2. Simulated Lipid Bilayer Systems with Varying Concentration of Additional Salt[a]

force field for lipids/ions	salt	[salt] mM	N_w	N_c	t_{sim} (ns)	t_{anal} (ns)	files
OPLS3e[12]	NaCl	100	8880	16	1000	1000	52, 53
	NaCl	200	8880	32	1000	1000	54, 55
	NaCl	500	8880	80	1000	900	56, 57
	NaCl	1000	8880	160	1000	900	58, 59
	$CaCl_2$	50	8880	8	1000	500	60, 61
	$CaCl_2$	100	8880	16	1000	250	62, 63
	$CaCl_2$	200	8880	32	1000	10 × 100	64, 65
	$CaCl_2$	500	8880	80	1000	10 × 100	66, 67
	$CaCl_2$	1000	8880	160	1000	10 × 100	68, 69
CHARMM36/NBFIX[4770]	NaCl	100	8880	16	500	475	71
	NaCl	200	8880	32	500	455	72
	NaCl	500	8880	80	500	440	73
	NaCl	1000	8880	160	500	485	74
	$CaCl_2$	50	8880	8	1000	850	75
	$CaCl_2$	100	8880	16	1000	850	76
	$CaCl_2$	200	8880	32	1000	750	77
	$CaCl_2$	500	8880	80	1000	850	78
	$CaCl_2$	1000	8726	158	1000	800	79

[a] N_w: Number of water molecules. N_c: Number of cations. t_{sim}: Total simulation time. t_{anal}: Time used for analysis. Files: Reference containing simulation files. Salt concentrations are calculated as [salt] = N_c×[water]/N_w, where [water] is 55.5 M.

salt concentrations (Table 2). Here we note just the key simulation details; all details are available in the run input files of the corresponding trajectories on Zenodo, see Tables 1 and 2 for the permanent links. Simulations used standard setup for planar bilayers, zero tension, and periodic boundary conditions in either Desmond, implemented in Schrödinger suite package version 2019.4[40,41] (OPLS3e) or in GROMACS version 2019.5[42] (CHARMM36). All simulated systems contained 200 POPC lipids (100 per leaflet) and they were generated using the system builder and model system regeneration tools of the Schrödinger software suite and the CHARMM-GUI Membrane builder, respectively. The NPT ensemble with temperature of 300 K and 1 atm pressure was used. In the simulations containing ions, ions were initially placed randomly in the water phase. Only the steady-state part of the simulations was analyzed, that is, after the bilayer area per lipid (A_L) stabilized and (in salt-containing systems) no further ions accumulated in the membrane. Plots of area per lipid as a function of time are available in Figure S13. Notably, the OPLS3e with high $CaCl_2$ concentration did not reach a steady state during 1 μs, so the simulation was divided into 10 × 100 ns parts analyzed separately. Details of the simulations with varying hydration levels are shown in Table 1 and with varying concentrations of additional salt in Table 2.

Starting Structures and Simulation Details. *OPLS3e.* Starting structures were constructed using the system builder and model system regeneration tools implemented in the Schrödinger software package.[40] The SPC water model[80] was used to solvate the systems. In addition, TIP3P[81] was used as a comparison in a few systems to ensure that the water model does not significantly influence the order parameters (see SI section 1 for details). For the dehydrated systems, excess water was removed from the starting structure of the full hydration system to attain the different hydration states. For the ion-containing systems, numbers of ions were calculated as N_c = [salt] × N_w/[water], where [water] = 55.5 M. The system with the strongest ion concentration (1 M) was constructed first using the system builder, and other concentrations were generated by randomly removing excess ions. Simulations were performed using Desmond in Schrödinger suite's package version 2019−4.[40,41] Default settings for membrane systems were used, with 2 fs time step and saving data every 10 ps; systems were relaxed before simulations with the default membrane relaxation protocol of Desmond. Temperature was set at 300 K and the system was kept in the NPT ensemble with the semi-isotropic Martyna−Tobias−Klein barostat[82] and the Nosé−Hoover-chain thermostat.[83]

CHARMM36. The starting structures were constructed using the CHARMM-GUI Membrane Builder (www.charmm-gui.org).[84] CHARMM TIP3P water model[85,86] was used to solvate the systems. Different hydration states were generated by removing excess water from the systems. Ions were added by using the `gmx genion` tool with `-np` and `-nn` flags in the GROMACS software package.[42] All simulations were performed with GROMACS version 2019.5.[42] Force field parameters were taken as in the CHARMM-GUI outputs; consequently, the NBFIX parameters[70] were used for ions. Simulations were performed with a 2 fs time step and data saved every 10 ps. Temperature of 300 K was maintained with the Nosé−Hoover thermostat,[87,88] and the semi-isotropic Parrinello−Rahman barostat[89] was used to control the pressure.

Analysis. The C−H bond order parameters S_{CH} were calculated directly using the eq 1. The S_{CH} of each C−H bond was gained by calculating first the S_{CH} of each individual lipid over time separately, and then calculating the average and the standard error of mean over different lipids. This analysis was performed using the Python program `calcOrderParameters.py` from NMRlipids GitHub;[90] the program uses the MDAnalysis library.[91,92] Number densities were obtained by using the `gmx density` tool in GROMACS software package.[42] Desmond files were converted for analysis into GROMACS format using VMD[93] for trajectories and `convert.py` by Intermol[94] for other files. After the `convert.py` conversion, names of the waters and ions, and representation of ions as individuals (instead of box of ions) were manually modified to match the other files.

https://doi.org/10.1021/acs.jcim.2c00395
J. Chem. Inf. Model. 2022, 62, 6462−6474

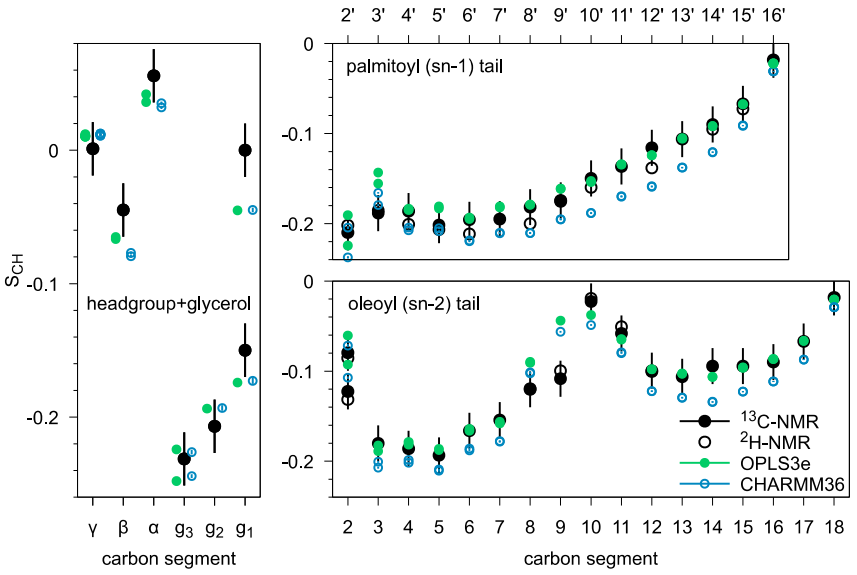

Figure 2. Carbon−hydrogen bond order parameters S_{CH} at full hydration for headgroup, backbone, and acyl chains in simulations and experiments. Experimental values for the POPC ^{1}H−^{13}C NMR at 300 K are from ref 17 and for ^{2}H NMR from ref 96. The ±0.02 error bars of the ^{13}C experimental values represent also the range within which most of the published experimental data resides, see discussion in text. For naming of carbon segments, see Figure 1.

The area per lipid A_L for each simulation frame was determined by calculating the area of the simulation box in the *xy*-plane and dividing that by the number of lipids per leaflet (n = 100); for the average A_L, only the equilibrated part of simulations (t_{anal}) was used.

The small-angle X-ray scattering (SAXS) form factors were calculated using the Python program `form_factor.py` in NMRlipids GitHub[95] and normalized by the first peak (located between 0.1 and 0.2 1/Å) height.

Lipid lateral diffusion coefficients D_L were determined from the slope of the mean squared displacement (MSD) of lipid centers of the mass. First the Gromacs tool `gmx trj` (with the `-nojump` and `-com` flags) was used to create trajectories of lipid centers of mass (for the equilibrated part of simulations t_{anal}, see Tables 1 and 2); then the tool `gmx msd` (with the `-lateral z` and `-rmcomm` flags) was used to calculate the MSD. The MSD was then plotted as a function of the displacement time, its linear region determined for each simulation, and D_L obtained as 0.25 × the slope (of a line fit to the linear region). For error estimation (visualized in Figure S14), the lipids were divided into five subgroups of equal size (n = 40), and MSDs calculated for each subgroup; the resulting five MSDs were treated as independent measurements, allowing the standard error of mean to be calculated for each displacement time; the steepest and gentlest slopes of lines that fit within these standard errors of the mean then provided error estimates for D_L.

RESULTS AND DISCUSSION

We calculated the C−H bond order parameters S_{CH}, see eq 1, from the simulations performed at different conditions, see Tables 1 and 2, with the OPLS3e and CHARMM36 force fields and compared them to the experimental S_{CH} available in the literature.

Validation against NMR Order Parameters: Full Hydration. Most S_{CH} produced by OPLS3e reside within ±0.02 from the experimental values, that is, within the estimated error range of NMR experiments (Figure 2). However, problems with S_{CH} magnitude occur in g_1, near the double bond of the sn-2 chain (C9), and at the start of sn-1 chain. For these regions the experimental error range is not reached with either of the force fields. Whereas OPLS3e and CHARMM36 produce almost identical S_{CH} for headgroup and glycerol backbone, the performance of OPLS3e for acyl chain regions seems to surpass CHARMM36.

In addition to magnitudes, a high-fidelity simulation model should produce correct forking pattern of S_{CH}. The term forking is used to describe the occurrence of unequal S_{CH} for different hydrogens attached to the same carbon, indicating different orientational populations of the two C−H bonds. It has been shown to not result from two separate populations of lipids.[97,98] Based on experimental data, most carbons of POPC have equally sampled C−H bond orientations and produce equal S_{CH} for both hydrogens; but there are few exceptions: the R and S hydrogens attached to the g_1 and g_3 carbons[17,97] in the glycerol backbone show in experiments significant and moderate forking, respectively, and the C2 carbon of sn-2 chain shows moderate forking, see Figure 2. An accurate force field should produce correct forking for g_1, g_3, and C2 but show no forking for other carbons. Forking is illustrated in the Figure 3 by angle distributions toward membrane normal. In CHARMM36 at full hydration, angle distributions for both hydrogens attached to the α carbon are equal (Figure 3A), but at 5 w/l (Figure 3B) distributions are unequal showing forking.

At full hydration, OPLS3e and CHARMM36 correctly produce forking for g_1 and g_3 and C2 of sn-2 chain. The C2 of sn-2 chain is of particular interest, as several force fields have been shown to struggle in this area.[3,22] However, both force fields produce forking for C2 and C3 at the start of sn-1 chain, which is not in agreement with the experimental data.

In general, OPLS3e produces very similar pattern of order parameters at full hydration as CHARMM36: close to experimental values but not within experimental accuracy. However, both force fields have problems with the correct description of g_1 at glycerol backbone, the beginning of the acyl tails, and the double bond of oleoyl chain. Therefore, we

https://doi.org/10.1021/acs.jcim.2c00395
J. Chem. Inf. Model. 2022, 62, 6462−6474

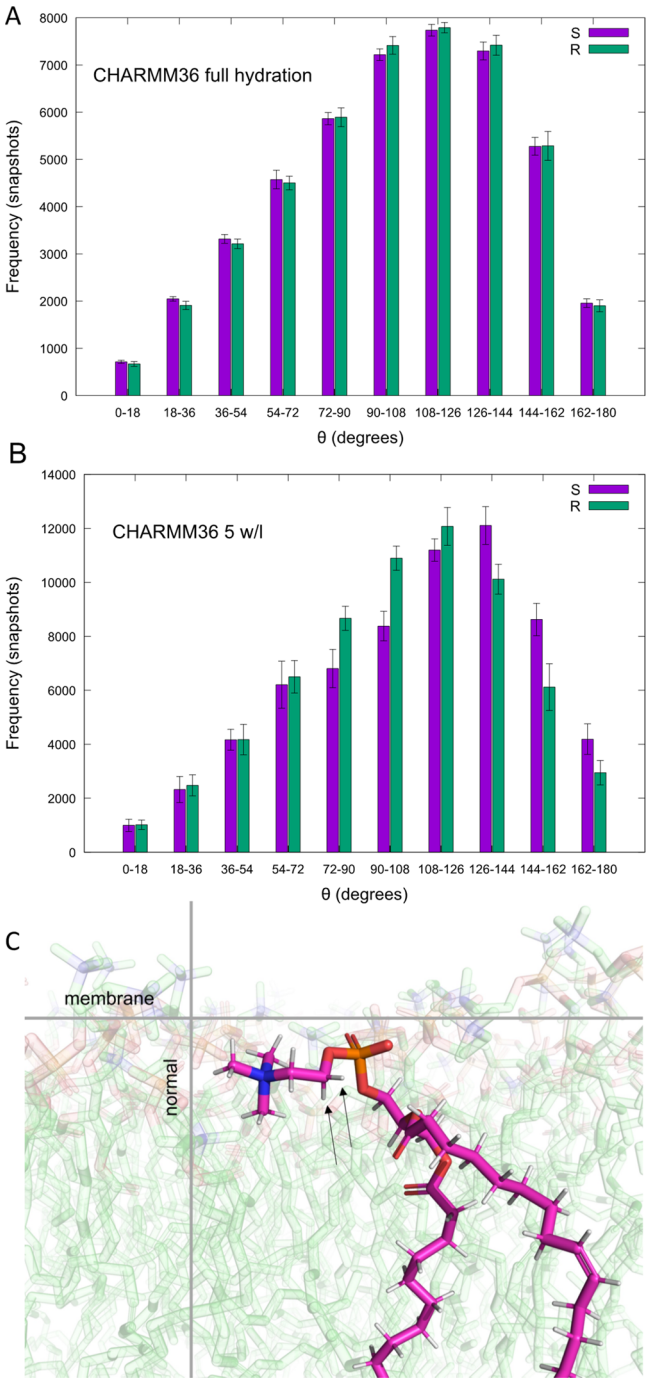

Figure 3. Illustration of forking. The θ-angle distribution of the α-carbon C−H bonds for R and S hydrogens (A) in CHARMM36 at full hydration (44 w/l) showing no forking and (B) in CHARMM36 at 5 w/l showing forking, cf. Figure 4. Distributions are calculated over 5 lipids as an example; error bars represent standard error of mean. θ is the angle between a C−H bond and the membrane normal; see Methods for more information. (C) A snapshot with the α-carbon hydrogens marked with arrows.

can conclude that OPLS3e produces comparable S_{CH} to CHARMM36 at full hydration, suggesting that structural description of POPC is similar and reasonably accurate in these force fields.

Validation against NMR Order Parameters: Dehydration. To examine how decreasing hydration affects the performance of OPLS3e, we compared the headgroup order parameters S^{β}_{CH} and S^{α}_{CH} from OPLS3e and CHARMM36 simulations against experimental NMR data (Figure 4). In experiments, S^{β}_{CH} and S^{α}_{CH} rise when hydration level drops, a change that should be captured in simulations. Although the S^{β}_{CH} are not within ±0.02 from experimental data (Figure 4), which indicates that neither force field exactly produces the atomistic resolution structural ensemble of the headgroup, the changes produced in S^{β}_{CH} and S^{α}_{CH} are qualitatively in line with experimental data: Both increase as hydration level decreases in OPLS3e, and in CHARMM36. Also, the magnitude of the rise for S^{α}_{CH} in OPLS3e aligns with the experimentally measured rise, but for S^{β}_{CH} the rise is exaggerated. Similar observations can be made with CHARMM36; however, an additional forking not reported in previous studies is occurring in CHARMM36 at the low hydration level of 5 w/l, see Figures 3 and 4. Our simulation length at 5 w/l (1000 ns, see Table 1) was reasonably long compared to earlier simulation studies reporting S^{β}_{CH} and S^{α}_{CH} at low hydration,[21] resulting in small error estimates and making the difference between the C−H bonds clearly visible.

Based on these data, structural response to dehydration seems quite realistic for the headgroup in OPLS3e. Botan et al. suggest an intuitive explanation for the rising headgroup order parameters to be that the choline headgroup orients more parallel to the membrane as the interlamellar space shrinks in response to the decreasing hydration level.[21] To conclude, in response to dehydration, OPLS3e does not produce atomistic resolution but its performance is very similar to CHARMM36 and headgroup orientation in OPLS3e can be thought to be reasonably accurate under dehydrated conditions. Although many currently available force fields produce qualitatively correct response to lowering hydration, OPLS3e and CHARMM36 seem to be among the most realistic considering the magnitude of the response.

Validation against NMR Order Parameters: Ions. Order parameters of the phosphatidylcholine (PC) headgroup C−H bonds can be used to compare ion binding to lipid membranes in experiments and simulations.[28] Charged objects on a PC bilayer interface induce systematic changes for the order parameters of the α and β carbons: A positive charge induces a decrease, and a negative charge an increase in S^{β}_{CH} and S^{α}_{CH}; a lack of change in S^{β}_{CH} and S^{α}_{CH} implies that the charged object does not bind to the PC bilayer interface. The concept, often referred to as the "molecular electrometer", has a strong experimental background[100] and Catte et al. have demonstrated that also in atomistic MD simulations, the S^{β}_{CH} and S^{α}_{CH} act as a direct indicator for bound cation charge.[28] Therefore, comparison of ion affinities between experiments and simulations based on the PC headgroup order parameters is possible, and allows the assessment of simulation model quality at different salt concentrations.

In the experiments, adding NaCl induces minimal decrease to S^{α}_{CH} and $S^{\beta}_{CH,}$ suggesting minimal Na^+ binding to membrane.[101] Several MD force fields overestimate Na^+ binding, and consequently S^{α}_{CH} and S^{β}_{CH} drop significantly more than in the experiments.[28] Based on the headgroup order parameter change (Figure 5 left panels) and ion distributions (Figure 6) in our simulations, OPLS3e is not an exception: Na^+ binding is overestimated. Notable is that overestimation is visible also at lower concentrations, near the physiological 150 mM concentration, that have the highest relevance in life sciences. Shapes of the order parameter curves in response to rising concentration of NaCl are very similar in OPLS3e and

https://doi.org/10.1021/acs.jcim.2c00395
J. Chem. Inf. Model. 2022, 62, 6462−6474

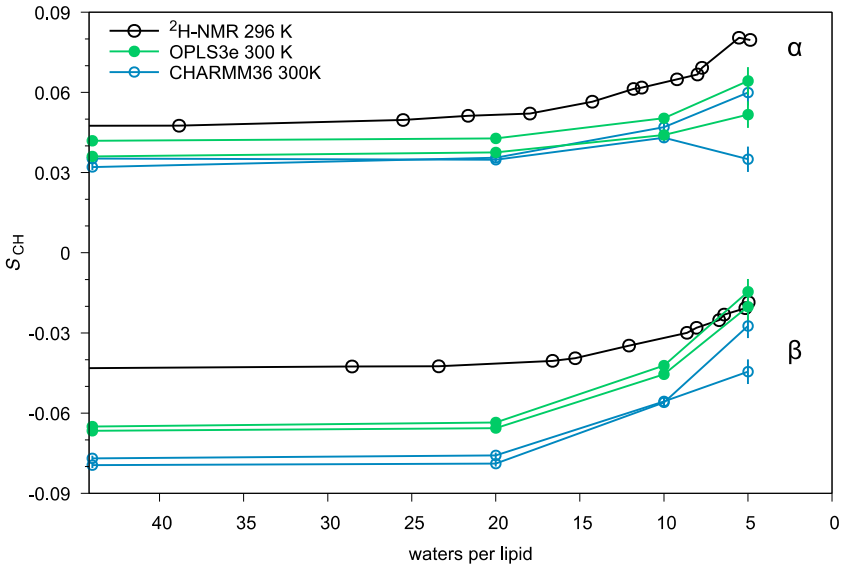

Figure 4. Response of the headgroup order parameters S^{β}_{CH} and S^{α}_{CH} to decreasing hydration level. Experimental values for POPC (^{2}H NMR) at 296 K are from ref 99. Notably, small changes in temperature seem not to have a major effect on S_{CH}, see Figures S10 and S11.

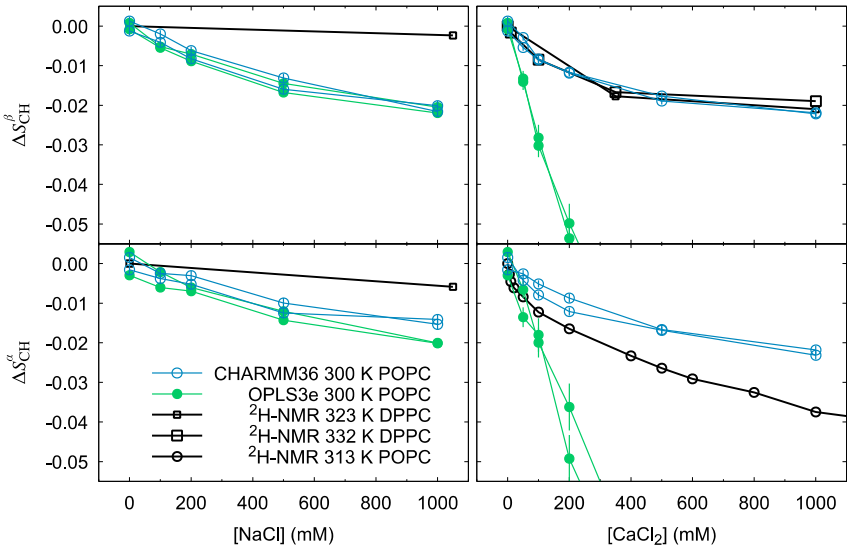

Figure 5. Change of order parameters in the headgroup α (lower panels) and β (upper panels) segments in response to rising concentrations of NaCl (left panels) or $CaCl_2$ (right panels). Experimental values for DPPC (^{2}H NMR) at 323 and 332 K are from ref 101 and for POPC (^{2}H NMR) at 313 K from ref 102. The out-of-bounds ΔS^{β}_{CH} points of OPLS3e in response to $CaCl_2$ (top right panel) are −0.102 ± 0.0085 and −0.089 ± 0.0090 (500 mM), and −0.13 ± 0.011 and −0.11 ± 0.013 (1000 mM). Corresponding values for ΔS^{α}_{CH} (bottom right panel) are −0.10 ± 0.010 and −0.093 ± 0.010 (500 mM), and −0.073 ± 0.016 and −0.097 ± 0.015 (1000 mM). Full figure is shown as the Figure S3. Due to their very slow equilibration (see Figure S4), for the OPLS3e $CaCl_2$ 200, 500, and 1000 mM concentrations the last 100 ns of the 1 μs simulation was used here. Note that to show possible forking at [salt] = 0, best seen in the bottom left panel for the OPLS3e, the average of the C−H bond order parameters of the R and S hydrogens was used to set the baseline.

CHARMM36 (Figure 5 left panels). Also, distributions of Na^+ and Cl^- seem highly similar (Figure 6), which suggests similar response to rising concentrations of NaCl in both force fields. For CHARMM36, we have included the nonbonded fix (NBFIX) corrections for ion parameters that have been suggested to recover overestimation of Na^+ binding;[103] however, the NBFIX-corrected CHARMM36 still appears to overestimate Na^+ binding (Figure 5. left panels).

Distributions of Na^+ and Cl^- (Figure 6) show that at lower salt concentrations (100 and 200 mM) ions are not only accumulated in the vicinity of the membrane, but they are also unevenly distributed in the bulk solution (Na^+ and Cl^- curves do not converge in the bulk); meaning that even with the rather large water/lipid ratios used here, the desired effect of having equal concentrations of both ions in the bulk solution is not reached in either of the force fields with [NaCl] < 500 mM.

Contrary to Na^+ ions, divalent Ca^{2+} ions bind significantly to lipid bilayers in experiments and the PC headgroup order parameters decrease when $CaCl_2$ concentration increases. Correct description of calcium binding to bilayers has proven to be challenging, and it seems that of the current force fields only the ECC-POPC model produces a quantitatively accurate response.[23,28,32] However, many force fields can have

https://doi.org/10.1021/acs.jcim.2c00395
J. Chem. Inf. Model. 2022, 62, 6462−6474

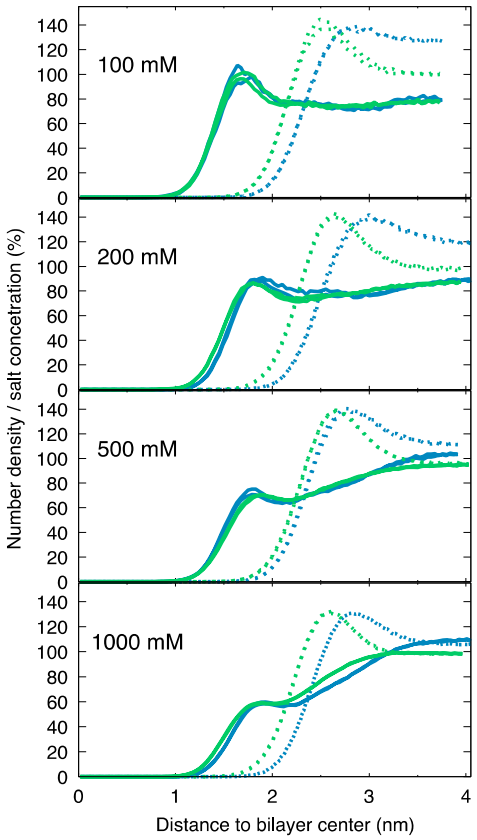

Figure 6. Distribution for Na^+ (solid lines) and Cl^- (dashed) ions along the bilayer normal shown as percentage of salt concentration. Green represents OPLS3e and blue CHARMM36. The graphs were obtained by dividing the number densities with the total salt concentration. Note that both leaflets are plotted (two almost fully overlapping lines) to highlight the symmetry of the ion distributions.

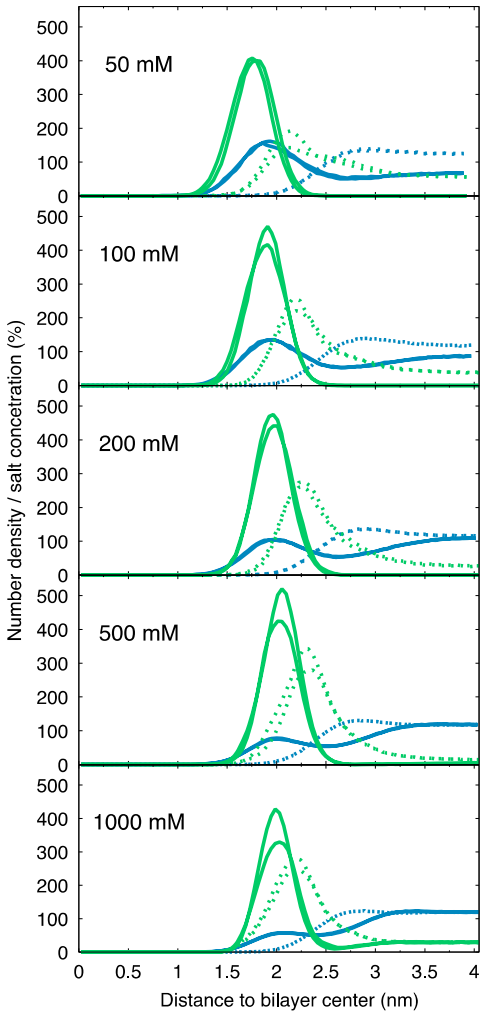

Figure 7. Distribution for Ca^{2+} (solid lines) and Cl^- (dashed lines) ions along the bilayer normal shown as percentage of salt concentration. Green represents OPLS3e and blue CHARMM36. The graphs were obtained by dividing the number densities with the total salt concentration. Because of their very slow equilibration (see Figure S4), for the OPLS3e $CaCl_2$ 200, 500, and 1000 mM concentrations the last 100 ns of the 1 μs simulation was used here. Note that both leaflets are plotted (two mostly overlapping lines).

qualitatively right response to Ca^{2+}, but overestimate the binding affinity. OPLS3e too produces qualitatively right order parameter response to Ca^{2+} ions: S^{β}_{CH} and S^{α}_{CH} decrease with rising concentration of Ca^{2+}; but the decrease is far too great (Figure 5 right panels) and binding of Ca^{2+} is highly overestimated (Figure 7). Order parameters of CHARMM36 are closer to experimental data than OPLS3e, suggesting that OPLS3e produces a poorer response to additional $CaCl_2$ than CHARMM36. However, S^{α}_{CH} of CHARMM36 suggest a slight underestimation of Ca^{2+} binding, and the NaCl and $CaCl_2$ responses seem very much alike, suggesting that—as already previously indicated in the SI of ref 23—CHARMM36 with NBFIX parameters does not distinguish the difference between monovalent Na^+ and divalent Ca^{2+} seen in the experiments.

Overestimation of ion binding in OPLS3e can be seen also in ion distributions, especially for $CaCl_2$ (Figure 7). Membrane pulls all calcium ions from the solution at low (≤200 mM) concentrations (and nearly all at higher concentrations), leaving no Ca^{2+} ions to the bulk. A high density of Ca^{2+} ions can be seen at the membrane surface, and consequently, the neutral PC bilayer will appear as positively charged, pulling a high density of Cl^- ions next to the Ca^{2+}. This charge layering will result in a strong electrostatic gradient. Such an artificially charged membrane can distort MD simulation results; in addition to effects on membrane behavior, influence on charged domains of membrane proteins is also conceivable, and might underlie some contradicting MD simulation results.[104,105] Therefore, extreme caution should be exercised when simulating membrane protein systems containing ions using force fields that are known to overestimate cation binding.

It is worth keeping in mind that as calcium binding of OPLS3e is so highly overestimated that (nearly) all Ca^{2+} is bound to bilayer, and no Ca^{2+} is left to solution, studying effects of calcium solutions on systems containing membranes using OPLS3e will be very difficult.

To conclude, additional NaCl produces similar response in both OPLS3e and CHARMM36: Slight overestimation of sodium binding compared to the minimal binding suggested by experimental data. On the contrary, responses to $CaCl_2$ differ in our MD simulation between OPLS3e and CHARMM36. OPLS3e produces qualitatively right response to rising $CaCl_2$ concentration, but radically overestimates the Ca^{2+} binding. Response of CHARMM36 seems to be closer to the experiments, although it is not able to reproduce the difference

https://doi.org/10.1021/acs.jcim.2c00395
J. Chem. Inf. Model. 2022, 62, 6462−6474

between Na^+ and Ca^{2+} ions. The commonly occurring overestimation of cation binding poses one of the biggest problems in current membrane modeling using MD simulations as it may result in positively charged membrane which can qualitatively distort the results.

Several strategies to fix the overbinding of ions to membranes have been proposed in the literature. NBFIX, which was used for CHARMM36 in this study, addresses the issue by tuning nonbonded parameters for specific atom pairs separately instead of using the standard arithmetic combining rule.[70] An alternative solution is the electronic continuum correction (ECC) strategy, which takes electronic polarization effects of solvent into account by scaling the charge of the ions.[29,32] We tested a similar scaling as in the ECC model for NaCl and $CaCl_2$ in OPLS3e which, prescaling, overestimates Na^+ and Ca^{2+} binding to membrane (Figure 5). Scaling of charge by 0.75 for Na^+ and Cl^- ions decreased Na^+ binding to membrane, and order parameters were closer to experimental values (than without scaling, see Figure S6). For $CaCl_2$, a similar simple scaling of ionic charges did not fix the surplus ion binding to the membrane (Figures S7 and S8). In the ECC-POPC model[32] scaling of both ions and the partial charges of lipid headgroup atoms was conducted, resulting in one of the most realistic force fields for lipids so far, since it can produce accurate binding also for divalent Ca^{2+} which, as already previously stated, has been very challenging with all current force fields.

For both force fields used in this study, OPLS3e and CHARMM36, new releases have been published recently. OPLS4 was published in 2021, with updates, e.g., on the representation of hydration and treatment of molecular ions.[106] There were, however, no changes in membrane parametrization. New CHARMM36 parameters called as C36/LJ-PME were also published in 2021,[25] with parameters optimized for lipid membranes using a semiautomated approach and including long-range dispersion via Lennard-Jones particle-mesh Ewald (LJ-PME). Order parameters were used as one of the optimization targets and, based on ref 25, order parameters for headgroup and tails of DPPC and DMPC lipids at full hydration align rather well with the experimental data. It will be interesting to see if these new updates offer improved performance for membranes especially in the presence of ions, which has been challenging area to be simulated correctly by the earlier force fields.

Applications: Responses of Area Per Lipid to Hydration and Ions. Area per lipid (A_L) is one of the most intuitive descriptors of a lipid bilayer, and thus one of the most common choices when force fields are validated against experimental data.[8,9] However, A_L cannot be directly measured experimentally, which complicates the exact comparison of experiments and simulations. For validation purposes, a direct comparison to the (X-ray and neutron) scattering form factors—which reflect the A_L and other membrane properties such as the bilayer thickness—is, thus, preferable.[3] Figure 8A presents such comparison of our OPLS3e and CHARMM36 simulations at full hydration against the small-angle X-ray scattering (SAXS) form factor of Kučerka et al.;[107] it is seen that while neither force field perfectly captures the membrane dimensions (e.g., CHARMM36 slightly misses the location of $F(q_z) = 0$ between 0.25 and 0.30 1/Å, OPLS3e is somewhat off at short wave vector lengths (q_z < 0.15 1/Å), and both force fields overestimate the relative height of the lobe located between 0.3 and 0.4 1/Å), they do reproduce the experimental

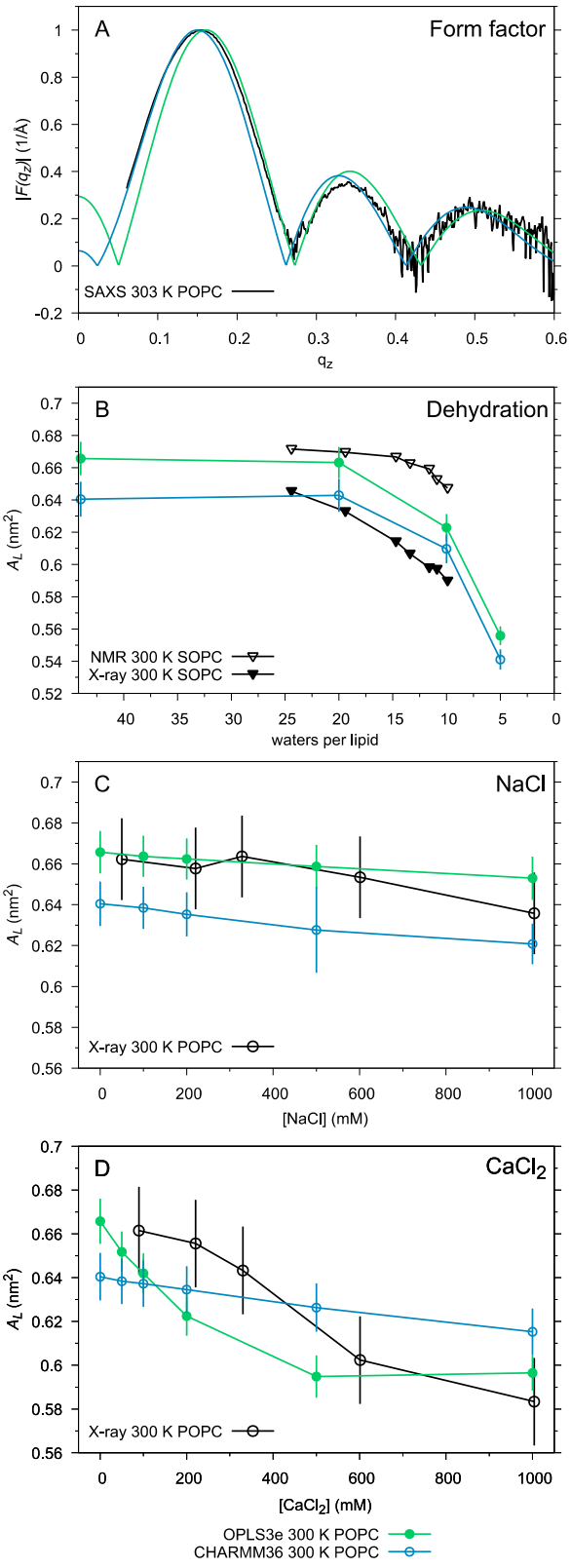

Figure 8. (A) Small-angle X-ray scattering (SAXS) form factors at full hydration (44 w/l); experimental data from ref 107. The responses of area per lipid A_L to lowering hydration level (B), added NaCl (C), and added $CaCl_2$ (D); error bars represent standard deviation. Experimental A_L as a function of lowering hydration for SOPC (NMR and X-ray) are from ref 109 and as a function of [NaCl] and [$CaCl_2$] for POPC from ref 110.

https://doi.org/10.1021/acs.jcim.2c00395
J. Chem. Inf. Model. 2022, 62, 6462−6474

form factor quite well. This is in line with the fact that our calculated full hydration A_L (0.666 ± 0.010 nm^2 in OPLS3e and 0.640 ± 0.011 nm^2 in CHARMM36) are well within the range of values reported in the experimental literature for POPC close to our simulation temperature of 300 K: This spans from 0.593 nm^2 (^{2}H NMR, 301 K, ref 108) to 0.683 nm^2; (X-ray scattering, 303 K, ref 107).

Instead of attempting quantitative comparisons of A_L, it is interesting to perform qualitative comparisons against experimentally observed responses in A_L with changing conditions. Figure 8B shows that A_L drops similarly in response to lowering hydration in our POPC simulations as what was experimentally[109] observed for SOPC (1-stearoyl-2-oleoyl-phosphatidylcholine) lipid bilayers (Figure 8B). The experimental data were only available for limited w/l ratios, but the magnitude of the drop in simulations correlates relatively well with experimental data in the available range; this indicates that OPLS3e and CHARMM36 capture rather well not only the PC headgroup behavior (Figure 4) but also the dehydration-associated changes in bilayer dimensions.

With additional NaCl, A_L do not change significantly at submolar concentrations in either experiments or simulations; both force fields, however, do reproduce the gently descending trend (Figure 8C) despite their overestimation of the headgroup response (Figure 5). With additional $CaCl_2$, A_L shows a significant drop within the experimentally studied concentrations (Figure 8D); CHARMM36 seems to underestimate this, while in OPLS3e the magnitude of the drop is in line with the experimentally determined change. When the latter is, however, viewed in light of the massive overestimation of the headgroup response (Figure 5), resulting from exaggerated affinity for Ca^{2+} (Figure 7), and the below-discussed overestimation of decrease in lateral diffusion, it is highly likely to result from a fortuitous cancellation of errors.

Applications: Lateral Diffusion. As lipid diffusion along biomembranes occurs on time scales accessible in MD simulations, and the lateral diffusion coefficients D_L can be determined using several (e.g., fluorescence, electron paramagnetic resonance (EPR), or NMR spectroscopy) experiments, the D_L are often compared between simulations and experiments. Problematic for some of the experimental techniques (such as EPR and fluorescence methods) is the requirement of labeling probes, which may have an impact on diffusion rates, making interpretation of results more challenging.[9] As NMR methods do not require system modifications with probes, we here use NMR data as reference.

Our CHARMM36 simulations at full hydration produced D_L = 5.7 ± 0.3 × 10^{-12} m^2/s, well in agreement with the values observed in earlier studies[111,112] at similar (∼20 to ∼50 ns) displacement times; while for OPLS3e diffusion is slightly faster, D_L = 6.5 ± 0.4 × 10^{-12} m^2/s, it still appears somewhat slower than in NMR experiments, where D_L = 8.87 × 10^{-12} m^2/s at 298 K and 10.7 × 10^{-12} m^2/s at 303 K.[113] One must keep in mind, however, that correcting for the finite periodic size of the simulation could increase D_L by even 200% in CHARMM36.[114] Indeed, the finite-size correction[115] using a membrane shear viscosity of 50.7 mPas (Matti Javanainen, personal communication) provides an estimate of 15 × 10^{-12} m^2/s for CHARMM36. This is considerably faster than what is observed experimentally—an interesting discrepancy in the light that CHARMM36 does reproduce the conformational dynamics of POPC very well.[116]

Nevertheless, as accurate determination of D_L from simulations is well-known[9] to be sensitive to various details, such as the simulation box size, measurement length, the observed displacement time, and the ability to apply corrections that in turn depend for example on the accurate determination of viscosity, we refrain from further quantitative study here. Instead, we turn to look at qualitative responses of D_L to changing conditions; here the observed trends should hold, if the membrane viscosity can be considered constant.

Figure 9A shows that response of diffusion to lowering hydration is qualitatively correct in both OPLS3e and CHARMM36: D_L drops significantly. However, the response begins later (at lower hydration levels) in simulations (<20 w/l) than in experiments (<40 w/l).

The two bottom panels in Figure 9 show the relative (normalized by the salt-free D_L) response of D_L to added NaCl (Figure 9B) and $CaCl_2$ (Figure 9C). The gray boxes in both panels indicate the reported experimental change: For [NaCl] below 270 mM a decrease of less than 3% was observed and for [$CaCl_2$] below 100 mM a decrease of less than 10%;[117] this suggests that at such concentrations of NaCl or $CaCl_2$ do not have major effect on lipid movements. In our simulations, additional NaCl in the experimental range (<270 mM) did not cause a decrease of D_L in either force field—but rather an increase, especially in CHARMM36 (Figure 9B). A similar increase was observed in CHARMM36 also with added $CaCl_2$ (Figure 9C), in line with the finding that the NBFIX parameters result in similar binding behavior for Ca^{2+} as for Na^+ (see Figures 5−7). In OPLS3e, however, additional $CaCl_2$ induced a significant drop of D_L (Figure 9C), in line with the distortedly strong Ca^{2+} binding (see Figures 5 and 7). This Ca^{2+}-induced suppression of movement of neutral POPC lipids in OPLS3e appears, in fact, to be as strong as what Filippov et al. reported (in the same salt concentration range) for the negatively charged DOPG (dioleoylphosphatidylglycerol) lipids, for which they observed an up-to-37% decrease in D_L upon cation binding.[117]

CONCLUSIONS

MD simulations using accurate force fields allow studying biomembranes at different conditions to interpret experimental results and to get knowledge of membrane structure, as well as the function and dynamics of membrane-bound proteins. Here, we demonstrate the performance of OPLS3e to be reasonably accurate for POPC membranes at full hydration and upon dehydration: The C−H bond order parameters produced with OPLS3e behave similarly to the well-established membrane force field CHARMM36 and closely follow the experimental observations. We also demonstrate that, in the absence of salt, OPLS3e simulation of a fully hydrated POPC bilayer produces the experimentally observed small-angle X-ray scattering form factor as well as an area per lipid that is well within the experimentally reported range. However, extreme caution should be exercised with systems containing ions, especially Ca^{2+} ions: OPLS3e, similarly to most other force fields, overestimates the binding of the cationic ions to the membrane, which both disrupts the neutral net charge of the membrane surface and changes the concentration of ions in the surrounding solvent. These issues could affect, for example, the structure and dynamics of the charged domains of membrane-bound proteins in unexpected ways.

Our results confirm that OPLS3e can be used for reliable MD simulations with simple POPC bilayers. Future studies

https://doi.org/10.1021/acs.jcim.2c00395
J. Chem. Inf. Model. 2022, 62, 6462−6474

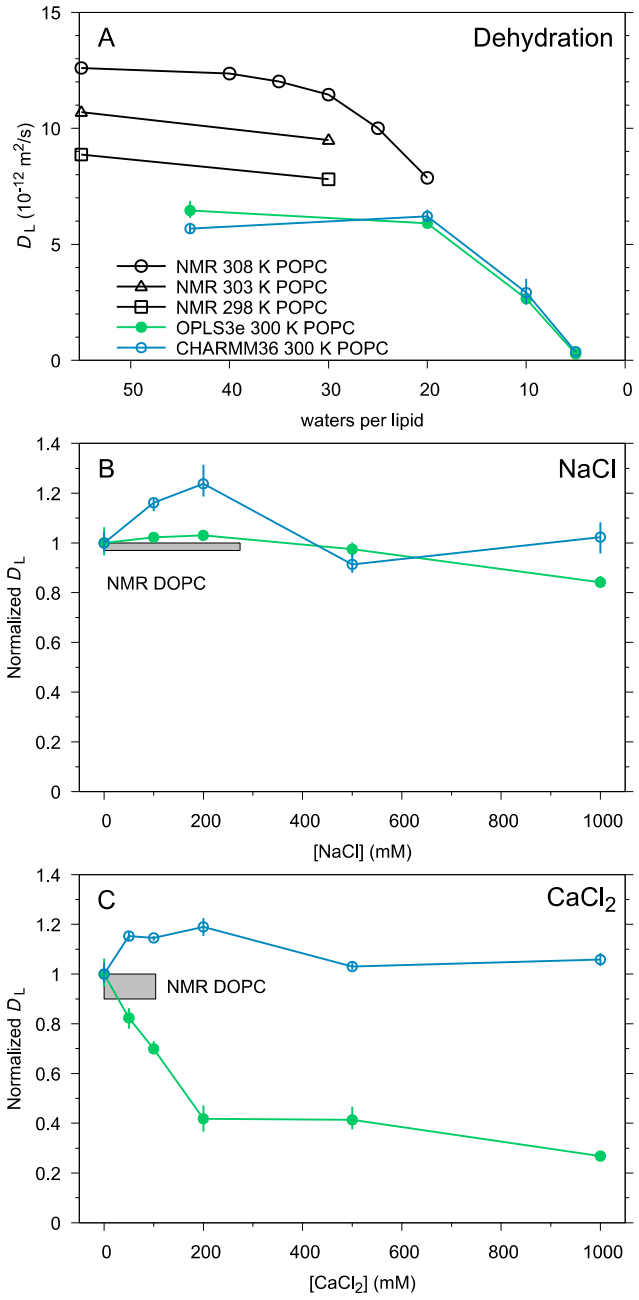

Figure 9. Responses of lipid lateral diffusion coefficients D_L to lowering hydration level (A), added NaCl (B), and added $CaCl_2$ (C). The experimental data in panel A are from ref 113, except for the 30 w/l values for 303 and 298 K, which are from ref 118. Note that panels B and C show D_L normalized with respect to the salt-free state, as the relevant experimental data in ref 117 were given as maximal percentage changes (indicated here with the gray rectangles).

should elucidate its performance with more diverse bilayers, such as ones containing mixtures of different lipids or cholesterol.

■ ASSOCIATED CONTENT

Supporting Information

The Supporting Information is available free of charge at https://pubs.acs.org/doi/10.1021/acs.jcim.2c00395.

Additional details of the impact of TIP3P water model in OPLS3e, order parameters in response to additional salt, equilibration times of the ion binding and impact on order parameters, scaling the ion charge in OPLS3e, small bug in CHARMM36 parameters, effect of temperature change in CHARMM36, and area per lipid as a function of time and lipid mean squared displacement (MSD) (PDF)

■ AUTHOR INFORMATION

Corresponding Author

Piia Bartos − *School of Pharmacy, University of Eastern Finland, 70211 Kuopio, Finland;* orcid.org/0000-0001-6002-1856; Email: piia.bartos@uef.fi

Authors

Milla Kurki − *School of Pharmacy, University of Eastern Finland, 70211 Kuopio, Finland;* orcid.org/0000-0001-8311-6057

Antti Poso − *School of Pharmacy, University of Eastern Finland, 70211 Kuopio, Finland;* orcid.org/0000-0003-4196-4204

Markus S. Miettinen − *Department of Chemistry and Computational Biology Unit, Department of Informatics, University of Bergen, 5007 Bergen, Norway;* orcid.org/0000-0002-3999-4722

Complete contact information is available at: https://pubs.acs.org/10.1021/acs.jcim.2c00395

Author Contributions

‡P.B. and M.S.M. contributed equally. A.P., P.B., and M.S.M. came up with the research idea. M.L. conducted the simulations and analysis under the supervision of A.P., P.B., and M.S.M. All authors contributed to the writing of the manuscript and have given approval to the final version of the manuscript.

Funding

M.L., A.P., and P.B. received funding from Finnish Cultural Foundation, the UEF Doctoral Programme, and competitive funding to strengthen university research profiles, 5th call, funding to University of Eastern Finland, funded by the Academy of Finland, funding decision nro 325022.

Notes

The authors declare no competing financial interest.

The scripts for the bond order parameter analysis are freely available at NMRlipids GitHub (https://github.com/NMRLipids) and the analyzed trajectories are permanently freely available at Zenodo (https://zenodo.org/).

■ ACKNOWLEDGMENTS

The authors thank CSC—IT Center for Science, Finland, for computational resources. M.S.M. thanks Matti Javanainen for helpful discussions concerning lipid lateral diffusion.

■ REFERENCES

(1) van Meer, G.; Voelker, D. R.; Feigenson, G. W. Membrane lipids: Where they are and how they behave. *Nat. Rev. Mol. Cell Biol.* **2008**, *9* (2), 112−124.

(2) Penke, B.; Paragi, G.; Gera, J.; Berkecz, R.; Kovács, Z.; Crul, T.; et al. The Role of Lipids and Membranes in the Pathogenesis of Alzheimer's Disease: A Comprehensive View. *Curr. Alzheimer Res.* **2018**, *15* (13), 1191−212.

(3) Ollila, O. H. S.; Pabst, G. Atomistic resolution structure and dynamics of lipid bilayers in simulations and experiments. *Biochimica*

et Biophysica Acta (BBA) - Biomembranes. **2016**, *1858* (10), 2512−2528.
(4) Róg, T.; Girych, M.; Bunker, A. Mechanistic Understanding from Molecular Dynamics in Pharmaceutical Research 2: Lipid Membrane in Drug Design. *Pharmaceuticals (Basel)* **2021**, *14* (10), 1062.
(5) Martinotti, C.; Ruiz-Perez, L.; Deplazes, E.; Mancera, R. L. Molecular Dynamics Simulation of Small Molecules Interacting with Biological Membranes. *ChemPhysChem* **2020**, *21* (14), 1486−1514.
(6) Muller, M. P.; Jiang, T.; Sun, C.; Lihan, M.; Pant, S.; Mahinthichaichan, P.; et al. Characterization of Lipid-Protein Interactions and Lipid-Mediated Modulation of Membrane Protein Function through Molecular Simulation. *Chem. Rev.* **2019**, *119* (9), 6086−6161.
(7) Dauber-Osguthorpe, P.; Hagler, A. T. Biomolecular force fields: where have we been, where are we now, where do we need to go and how do we get there? *J. Comput. Aided Mol. Des.* **2019**, *33* (2), 133−203.
(8) Lyubartsev, A. P.; Rabinovich, A. L. Force Field Development for Lipid Membrane Simulations. *Biochimica et Biophysica Acta (BBA) - Biomembranes.* **2016**, *1858* (10), 2483−2497.
(9) Poger, D.; Caron, B.; Mark, A. E. Validating lipid force fields against experimental data: Progress, challenges and perspectives. *Biochim. Biophys. Acta* **2016**, *1858* (7), 1556−1565.
(10) Beauchamp, K. A.; Lin, Y. S.; Das, R.; Pande, V. S. Are Protein Force Fields Getting Better? A Systematic Benchmark on 524 Diverse NMR Measurements. *J. Chem. Theory Comput.* **2012**, *8* (4), 1409−1414.
(11) Chu, H.; Cao, L.; Peng, X.; Li, G. Polarizable force field development for lipids and their efficient applications in membrane proteins. *WIREs Computational Molecular Science.* **2017**, *7* (5), No. e1312.
(12) Roos, K.; Wu, C.; Damm, W.; Reboul, M.; Stevenson, J. M.; Lu, C.; et al. OPLS3e: Extending Force Field Coverage for Drug-Like Small Molecules. *J. Chem. Theory Comput.* **2019**, *15* (3), 1863−1874.
(13) Harder, E.; Damm, W.; Maple, J.; Wu, C.; Reboul, M.; Xiang, J. Y.; et al. OPLS3: A Force Field Providing Broad Coverage of Drug-like Small Molecules and Proteins. *J. Chem. Theory Comput.* **2016**, *12* (1), 281−296.
(14) Seelig, J. Deuterium magnetic resonance: theory and application to lipid membranes. *Q. Rev. Biophys.* **1977**, *10* (3), 353−418.
(15) Gross, J. D.; Warschawski, D. E.; Griffin, R. G. Dipolar Recoupling in MAS NMR: A Probe for Segmental Order in Lipid Bilayers. *J. Am. Chem. Soc.* **1997**, *119* (4), 796−802.
(16) Dvinskikh, S. V.; Castro, V.; Sandström, D. Efficient solid-state NMR methods for measuring heteronuclear dipolar couplings in unoriented lipid membrane systems. *Phys. Chem. Chem. Phys.* **2005**, *7* (4), 607−613.
(17) Ferreira, T. M.; Coreta-Gomes, F.; Ollila, O. H. S.; Moreno, M. J.; Vaz, W. L. C.; Topgaard, D. Cholesterol and POPC segmental order parameters in lipid membranes: solid state 1H−13C NMR and MD simulation studies. *Phys. Chem. Chem. Phys.* **2013**, *15* (6), 1976−1989.
(18) Klauda, J. B.; Venable, R. M.; Freites, J. A.; O'Connor, J. W.; Tobias, D. J.; Mondragon-Ramirez, C.; et al. Update of the CHARMM all-atom additive force field for lipids: validation on six lipid types. *J. Phys. Chem. B* **2010**, *114* (23), 7830−7843.
(19) Jämbeck, J. P. M.; Lyubartsev, A. P. Derivation and systematic validation of a refined all-atom force field for phosphatidylcholine lipids. *J. Phys. Chem. B* **2012**, *116* (10), 3164−3179.
(20) Dickson, C. J.; Madej, B. D.; Skjevik, ÅA; Betz, R. M.; Teigen, K.; et al. Lipid14: The Amber Lipid Force Field. *J. Chem. Theory Comput.* **2014**, *10* (2), 865−879.
(21) Botan, A.; Favela-Rosales, F.; Fuchs, P. F. J.; Javanainen, M.; Kanduč, M.; Kulig, W.; et al. Toward Atomistic Resolution Structure of Phosphatidylcholine Headgroup and Glycerol Backbone at Different Ambient Conditions. *J. Phys. Chem. B* **2015**, *119* (49), 15075−15088.
(22) Pezeshkian, W.; Khandelia, H.; Marsh, D. Lipid Configurations from Molecular Dynamics Simulations. *Biophys. J.* **2018**, *114* (8), 1895−1907.
(23) Antila, H.; Buslaev, P.; Favela-Rosales, F.; Ferreira, T. M.; Gushchin, I.; Javanainen, M.; et al. Headgroup Structure and Cation Binding in Phosphatidylserine Lipid Bilayers. *J. Phys. Chem. B* **2019**, *123* (43), 9066−9079.
(24) Bacle, A.; Buslaev, P.; Garcia-Fandino, R.; Favela-Rosales, F.; Mendes Ferreira, T.; Fuchs, P. F. J.; et al. Inverse Conformational Selection in Lipid-Protein Binding. *J. Am. Chem. Soc.* **2021**, *143* (34), 13701−13709.
(25) Yu, Y.; Krämer, A.; Venable, R. M.; Simmonett, A. C.; MacKerell, A. D.; Klauda, J. B.; et al. Semi-automated Optimization of the CHARMM36 Lipid Force Field to Include Explicit Treatment of Long-Range Dispersion. *J. Chem. Theory Comput.* **2021**, *17* (3), 1562−1580.
(26) Dickson, C. J.; Walker, R. C.; Gould, I. R. Lipid21: Complex Lipid Membrane Simulations with AMBER. *J. Chem. Theory Comput.* **2022**, *18* (3), 1726−1736.
(27) Grote, F.; Lyubartsev, A. P. Optimization of Slipids Force Field Parameters Describing Headgroups of Phospholipids. *J. Phys. Chem. B* **2020**, *124* (40), 8784−8793.
(28) Catte, A.; Girych, M.; Javanainen, M.; Loison, C.; Melcr, J.; Miettinen, M. S.; et al. Molecular electrometer and binding of cations to phospholipid bilayers. *Phys. Chem. Chem. Phys.* **2016**, *18* (47), 32560−32569.
(29) Kohagen, M.; Mason, P. E.; Jungwirth, P. Accounting for Electronic Polarization Effects in Aqueous Sodium Chloride via Molecular Dynamics Aided by Neutron Scattering. *J. Phys. Chem. B* **2016**, *120* (8), 1454−1460.
(30) Melcrová, A.; Pokorna, S.; Pullanchery, S.; Kohagen, M.; Jurkiewicz, P.; Hof, M.; et al. The complex nature of calcium cation interactions with phospholipid bilayers. *Sci. Rep.* **2016**, *6*, 38035.
(31) Javanainen, M.; Melcrová, A.; Magarkar, A.; Jurkiewicz, P.; Hof, M.; Jungwirth, P.; et al. Two cations, two mechanisms: interactions of sodium and calcium with zwitterionic lipid membranes. *Chem. Commun. (Camb).* **2017**, *53* (39), 5380−5383.
(32) Melcr, J.; Martinez-Seara, H.; Nencini, R.; Kolafa, J.; Jungwirth, P.; Ollila, O. H. S. Accurate Binding of Sodium and Calcium to a POPC Bilayer by Effective Inclusion of Electronic Polarization. *J. Phys. Chem. B* **2018**, *122* (16), 4546−4557.
(33) Knecht, V.; Marrink, S. Molecular Dynamics Simulations of Lipid Vesicle Fusion in Atomic Detail. *Biophysical Journal.* **2007**, *92* (12), 4254−4261.
(34) Kavalali, E. T. The mechanisms and functions of spontaneous neurotransmitter release. *Nat. Rev. Neurosci.* **2015**, *16* (1), 5−16.
(35) Magarkar, A.; Jurkiewicz, P.; Allolio, C.; Hof, M.; Jungwirth, P. Increased Binding of Calcium Ions at Positively Curved Phospholipid Membranes. *J. Phys. Chem. Lett.* **2017**, *8* (2), 518−523.
(36) Flood, E.; Boiteux, C.; Lev, B.; Vorobyov, I.; Allen, T. W. Atomistic Simulations of Membrane Ion Channel Conduction, Gating, and Modulation. *Chem. Rev.* **2019**, *119* (13), 7737−7832.
(37) Cordomi, A.; Edholm, O.; Perez, J. J. Effect of ions on a dipalmitoyl phosphatidylcholine bilayer. A molecular dynamics simulation study. *J. Phys. Chem. B* **2008**, *112* (5), 1397−1408.
(38) Cordomi, A.; Edholm, O.; Perez, J. J. Effect of Force Field Parameters on Sodium and Potassium Ion Binding to Dipalmitoyl Phosphatidylcholine Bilayers. *J. Chem. Theory Comput.* **2009**, *5* (8), 2125−2134.
(39) Ollila, S.; Miettinen, M. S.; Vogel, A. Accuracy of order parameter measurements. *Figshare*, 2015. DOI: 10.6084/m9.figshare.1577576.
(40) *Maestro*, release 2020-4; Schrödinger: New York, NY, 2020.
(41) Bowers, K. J.; Chow, E.; Xu, H.; Dror, R. O.; Eastwood, M. P.; Gregersen, B. A.; et al. Scalable Algorithms for Molecular Dynamics Simulations on Commodity Clusters. *SC '06: Proceedings of the 2006 ACM/IEEE Conference on Supercomputing* **2006**, 43.
(42) Abraham, M.; Murtola, T.; Schulz, R.; Páll, S.; Smith, J. C.; Hess, B. GROMACS: High performance molecular simulations

through multi-level parallelism from laptops to supercomputers. *SoftwareX* **2015**, *1-2*, 19−25.
(43) Lindström, M. MD simulation of POPC bilayer with OPLS3e force field. Full hydration 44 w/l. *Zenodo* **2022**, DOI: 10.5281/zenodo.6582985.
(44) Lindström, M. MD simulation of POPC bilayer with OPLS3e force field. 20 w/l. *Zenodo* **2022**, DOI: 10.5281/zenodo.6618786.
(45) Lindström, M. MD simulation of POPC bilayer with OPLS3e force field. 10 w/l. *Zenodo* **2022**, DOI: 10.5281/zenodo.6618793.
(46) Lindström, M. MD simulation of POPC bilayer with OPLS3e force field. 5 w/l. *Zenodo* **2022**, DOI: 10.5281/zenodo.6618796.
(47) Klauda, J. B.; Venable, R. M.; Freites, J. A.; O'Connor, J. W.; Tobias, D. J.; Mondragon-Ramirez, C.; et al. Update of the CHARMM all-atom additive force field for lipids: validation on six lipid types. *J. Phys. Chem. B* **2010**, *114* (23), 7830−7843.
(48) Lindström, M. MD simulation of POPC bilayer with CHARMM36 force field. Full hydration 44 w/l. *Zenodo* **2022**, DOI: 10.5281/zenodo.6336691.
(49) Lindström, M. MD simulation of POPC bilayer with CHARMM36 force field. 20 w/l. *Zenodo* **2022**, DOI: 10.5281/zenodo.6335769.
(50) Lindström, M. MD simulation of POPC bilayer with CHARMM36 force field. 10 w/l. *Zenodo* **2022**, DOI: 10.5281/zenodo.6334005.
(51) Lindström, M. MD simulation of POPC bilayer with CHARMM36 force field. 5 w/l. *Zenodo* **2022**, DOI: 10.5281/zenodo.6333548.
(52) Lindström, M. MD simulation of POPC bilayer with OPLS3e force field, 100 mM NaCl part 1. *Zenodo* **2022**, DOI: 10.5281/zenodo.6619578.
(53) Lindström, M. MD simulation of POPC bilayer with OPLS3e force field, 100 mM NaCl part 2. *Zenodo* **2022**, DOI: 10.5281/zenodo.6619589.
(54) Lindström, M. MD simulation of POPC bilayer with OPLS3e force field, 200 mM NaCl part 1. *Zenodo* **2022**, DOI: 10.5281/zenodo.6618822.
(55) Lindström, M. MD simulation of POPC bilayer with OPLS3e force field, 200 mM NaCl part 2. *Zenodo* **2022**, DOI: 10.5281/zenodo.6619563.
(56) Lindström, M. MD simulation of POPC bilayer with OPLS3e force field, 500 mM NaCl part 1. *Zenodo* **2022**, DOI: 10.5281/zenodo.6618810.
(57) Lindström, M. MD simulation of POPC bilayer with OPLS3e force field, 500 mM NaCl part 2. *Zenodo* **2022**, DOI: 10.5281/zenodo.6364498.
(58) Lindström, M. MD simulation of POPC bilayer with OPLS3e force field, 1000 mM NaCl part 1. *Zenodo* **2022**, DOI: 10.5281/zenodo.6618809.
(59) Lindström, M. MD simulation of POPC bilayer with OPLS3e force field, 1000 mM NaCl part 2. *Zenodo* **2022**, DOI: 10.5281/zenodo.6366287.
(60) Lindström, M. MD simulation of POPC bilayer with OPLS3e force field, 50 mM $CaCl_2$ part 1. *Zenodo* **2022**, DOI: 10.5281/zenodo.6618921.
(61) Lindström, M. MD simulation of POPC bilayer with OPLS3e force field, 50 mM $CaCl_2$ part 2. *Zenodo* **2022**, DOI: 10.5281/zenodo.6346717.
(62) Lindström, M. MD simulation of POPC bilayer with OPLS3e force field, 100 mM $CaCl_2$ part 1. *Zenodo* **2022**, DOI: 10.5281/zenodo.6618936.
(63) Lindström, M. MD simulation of POPC bilayer with OPLS3e force field, 100 mM $CaCl_2$ part 2. *Zenodo* **2022**, DOI: 10.5281/zenodo.6347982.
(64) Lindström, M. MD simulation of POPC bilayer with OPLS3e force field, 200 mM $CaCl_2$ part 1. *Zenodo* **2022**, DOI: 10.5281/zenodo.6618953.
(65) Lindström, M. MD simulation of POPC bilayer with OPLS3e force field, 200 mM $CaCl_2$ part 2. *Zenodo* **2022**, DOI: 10.5281/zenodo.6350600.
(66) Lindström, M. MD simulation of POPC bilayer with OPLS3e force field, 500 mM $CaCl_2$ part 1. *Zenodo* **2022**, DOI: 10.5281/zenodo.6618982.
(67) Lindström, M. MD simulation of POPC bilayer with OPLS3e force field, 500 mM $CaCl_2$ part 2. *Zenodo* **2022**, DOI: 10.5281/zenodo.6351089.
(68) Lindström, M. MD simulation of POPC bilayer with OPLS3e force field, 1000 mM $CaCl_2$ part 1. *Zenodo* **2022**, DOI: 10.5281/zenodo.6619080.
(69) Lindström, M. MD simulation of POPC bilayer with OPLS3e force field, 1000 mM $CaCl_2$ part 2. *Zenodo* **2022**, DOI: 10.5281/zenodo.6619202.
(70) Han, K.; Venable, R. M.; Bryant, A.; Legacy, C. J.; Shen, R.; Li, H.; et al. Graph−Theoretic Analysis of Monomethyl Phosphate Clustering in Ionic Solutions. *J. Phys. Chem. B* **2018**, *122* (4), 1484−1494.
(71) Lindström, M. MD simulation of POPC bilayer with CHARMM36 force field, 100 mM NaCl. *Zenodo* **2022**, DOI: 10.5281/zenodo.6342104.
(72) Lindström, M. MD simulation of POPC bilayer with CHARMM36 force field, 200 mM NaCl. *Zenodo* **2022**, DOI: 10.5281/zenodo.6342175.
(73) Lindström, M. MD simulation of POPC bilayer with CHARMM36 force field, 500 mM NaCl. *Zenodo* **2022**, DOI: 10.5281/zenodo.6342522.
(74) Lindström, M. MD simulation of POPC bilayer with CHARMM36 force field, 1000 mM NaCl. *Zenodo* **2022**, DOI: 10.5281/zenodo.6342652.
(75) Lindström, M. MD simulation of POPC bilayer with CHARMM36 force field, 50 mM $CaCl_2$. *Zenodo* **2022**, DOI: 10.5281/zenodo.6341899.
(76) Lindström, M. MD simulation of POPC bilayer with CHARMM36 force field, 100 mM $CaCl_2$. *Zenodo* **2022**, DOI: 10.5281/zenodo.6341420.
(77) Lindström, M. MD simulation of POPC bilayer with CHARMM36 force field, 200 mM $CaCl_2$. *Zenodo* **2022**, DOI: 10.5281/zenodo.6337813.
(78) Lindström, M. MD simulation of POPC bilayer with CHARMM36 force field, 500 mM $CaCl_2$. *Zenodo* **2022**, DOI: 10.5281/zenodo.6339898.
(79) Lindström, M. MD simulation of POPC bilayer with CHARMM36 force field, 1000 mM $CaCl_2$. *Zenodo* **2022**, DOI: 10.5281/zenodo.6337490.
(80) Berendsen, H. J. C.; Postma, J. P. M.; van Gunsteren, W. F.; Hermans, J. Interaction Models for Water in Relation to Protein Hydration. In *Intermolecular Forces*; Pullman, B., Ed. The Jerusalem Symposia on Quantum Chemistry and Biochemistry. Volume 14; Springer: Dordrecht, 1981; pp 331−342.
(81) Jorgensen, W. L.; Chandrasekhar, J.; Madura, J. D.; Impey, R. W.; Klein, M. L. Comparison of simple potential functions for simulating liquid water. *J. Chem. Phys.* **1983**, *79* (2), 926−935.
(82) Martyna, G. J.; Tobias, D. J.; Klein, M. L. Constant pressure molecular dynamics algorithms. *J. Chem. Phys.* **1994**, *101* (5), 4177−4189.
(83) Martyna, G. J.; Klein, M. L.; Tuckerman, M. Nosé−Hoover chains: The canonical ensemble via continuous dynamics. *J. Chem. Phys.* **1992**, *97* (4), 2635−2643.
(84) Jo, S.; Kim, T.; Iyer, V. G.; Im, W. CHARMM-GUI: A web-based graphical user interface for CHARMM. *J. Comput. Chem.* **2008**, *29* (11), 1859−1865.
(85) Durell, S. R.; Brooks, B. R.; Ben-Naim, A. Solvent-Induced Forces between Two Hydrophilic Groups. *J. Phys. Chem.* **1994**, *98* (8), 2198−2202.
(86) Neria, E.; Fischer, S.; Karplus, M. Simulation of activation free energies in molecular systems. *J. Chem. Phys.* **1996**, *105* (5), 1902−1921.
(87) Nosé, S. A molecular dynamics method for simulations in the canonical ensemble. *Mol. Phys.* **1984**, *52* (2), 255−268.

https://doi.org/10.1021/acs.jcim.2c00395
J. Chem. Inf. Model. 2022, 62, 6462−6474

(88) Hoover, W. G. Canonical dynamics: Equilibrium phase-space distributions. *Phys. Rev. A* **1985**, *31* (3), 1695−1697.
(89) Parrinello, M.; Rahman, A. Polymorphic transitions in single crystals: A new molecular dynamics method. *J. Appl. Phys.* **1981**, *52* (12), 7182−7190.
(90) NMRlipids collaboration. MATCH. *GitHub Repository*, 2018. github.com/NMRLipids/MATCH/blob/b7baf4550dde4e0f7c69db777db5dcca205973a2/scripts/calcOrderParameters.py.
(91) Michaud-Agrawal, N.; Denning, E. J.; Woolf, T. B.; Beckstein, O. MDAnalysis: a toolkit for the analysis of molecular dynamics simulations. *J. Comput. Chem.* **2011**, *32* (10), 2319−2327.
(92) Gowers, R. J.; Linke, M; Barnoud, J; Reddy, T. J. E.; Melo, M. N.; Seyler, S. L.; Domanski, J; Dotson, D. L.; Buchoux, S; Kenney, I. M.; Beckstein, O; Benthall, S.; Rostrup, S. MDAnalysis: A Python package for the rapid analysis of molecular dynamics simulations. *Proceedings of the 15th Python in Science Conference* **2016**, 98−105, DOI: 10.25080/majora-629e541a-00e.
(93) Humphrey, W.; Dalke, A.; Schulten, K. VMD} − {V}isual {M}olecular {D}ynamics. *Journal of Molecular Graphics.* **1996**, *14*, 33−38.
(94) Shirts, M. R.; Klein, C.; Swails, J. M.; Yin, J.; Gilson, M. K.; Mobley, D. L.; Case, D. A.; Zhong, E. D. Lessons learned from comparing molecular dynamics engines on the SAMPL5 dataset. *Journal Comput.-Aided Mol. Des.* **2017**, *31* (1), 147−161.
(95) NMRlipids collaboration. NMRlipids Databank. *Github Repository*, 2022. github.com/NMRlipids/Databank/blob/671596cb334d86a6f4e98d92d0578affbaf5feec/Scripts/AnalyzeDatabank/form_factor.py.
(96) Seelig, J.; Waespe-Sarcevic, N. Molecular order in cis and trans unsaturated phospholipid bilayers. *Biochemistry.* **1978**, *17* (16), 3310−3315.
(97) Gally, H. U.; Pluschke, G.; Overath, P.; Seelig, J. Structure of Escherichia coli membranes. Glycerol auxotrophs as a tool for the analysis of the phospholipid head-group region by deuterium magnetic resonance. *Biochemistry.* **1981**, *20* (7), 1826−1831.
(98) Engel, A. K.; Cowburn, D. The origin of multiple quadrupole couplings in the deuterium NMR spectra of the 2 chain of 1,2 dipalmitoyl-sn-glycero-3-phosphorylcholine. *FEBS Lett.* **1981**, *126* (2), 169−171.
(99) Bechinger, B.; Seelig, J. Conformational changes of the phosphatidylcholine headgroup due to membrane dehydration. A 2H-NMR study. *Chemistry and Physics of Lipids* **1991**, *58* (1-2), 1−5.
(100) Seelig, J.; Macdonald, P. M.; Scherer, P. G. Phospholipid head groups as sensors of electric charge in membranes. *Biochemistry.* **1987**, *26* (24), 7535−7541.
(101) Akutsu, H.; Seelig, J. Interaction of metal ions with phosphatidylcholine bilayer membranes. *Biochemistry.* **1981**, *20* (26), 7366−7373.
(102) Altenbach, C.; Seelig, J. Calcium binding to phosphatidylcholine bilayers as studied by deuterium magnetic resonance. Evidence for the formation of a calcium complex with two phospholipid molecules. *Biochemistry.* **1984**, *23* (17), 3913−3920.
(103) Venable, R. M.; Luo, Y.; Gawrisch, K.; Roux, B.; Pastor, R. W. Simulations of anionic lipid membranes: development of interaction-specific ion parameters and validation using NMR data. *J. Phys. Chem. B* **2013**, *117* (35), 10183−10192.
(104) Arkhipov, A.; Shan, Y.; Das, R.; Endres, N. F.; Eastwood, M. P.; Wemmer, D. E.; et al. Architecture and membrane interactions of the EGF receptor. *Cell.* **2013**, *152* (3), 557−569.
(105) Kaszuba, K.; Grzybek, M.; Orłowski, A.; Danne, R.; Róg, T.; Simons, K.; et al. N-Glycosylation as determinant of epidermal growth factor receptor conformation in membranes. *Proc. Natl. Acad. Sci. U. S. A.* **2015**, *112* (14), 4334−4339.
(106) Lu, C.; Wu, C.; Ghoreishi, D.; Chen, W.; Wang, L.; Damm, W. OPLS4: Improving Force Field Accuracy on Challenging Regimes of Chemical Space. *Journal of Chemical Theory and Computation* **2021**, *17* (7), 4291−4300.
(107) Kucerka, N.; Tristram-Nagle, S.; Nagle, J. F. Structure of fully hydrated fluid phase lipid bilayers with monounsaturated chains. *J. Membr. Biol.* **2006**, *208* (3), 193−202.
(108) Leftin, A.; Molugu, T. R.; Job, C.; Beyer, K.; Brown, M. F. Area per lipid and cholesterol interactions in membranes from separated local-field (13)C NMR spectroscopy. *Biophys. J.* **2014**, *107* (10), 2274−2286.
(109) Koenig, B. W.; Strey, H. H.; Gawrisch, K. Membrane lateral compressibility determined by NMR and x-ray diffraction: effect of acyl chain polyunsaturation. *Biophys. J.* **1997**, *73* (4), 1954−1966.
(110) Pabst, G.; Hodzic, A.; Strancar, J.; Danner, S.; Rappolt, M.; Laggner, P. Rigidification of neutral lipid bilayers in the presence of salts. *Biophys. J.* **2007**, *93* (8), 2688−2696.
(111) Piggot, T. J.; Piñeiro, Á; Khalid, S. Molecular Dynamics Simulations of Phosphatidylcholine Membranes: A Comparative Force Field Study. *J. Chem. Theory Comput.* **2012**, *8* (11), 4593−4609.
(112) Pluhackova, K.; Kirsch, S. A.; Han, J.; Sun, L.; Jiang, Z.; Unruh, T.; et al. A Critical Comparison of Biomembrane Force Fields: Structure and Dynamics of Model DMPC, POPC, and POPE Bilayers. *J. Phys. Chem. B* **2016**, *120* (16), 3888−3903.
(113) Filippov, A.; Orädd, G.; Lindblom, G. Influence of Cholesterol and Water Content on Phospholipid Lateral Diffusion in Bilayers. *Langmuir* **2003**, *19* (16), 6397−6400.
(114) Venable, R. M.; Ingólfsson, H. I.; Lerner, M. G.; Perrin, B. S.; Camley, B. A.; Marrink, S. J.; et al. Lipid and Peptide Diffusion in Bilayers: The Saffman-Delbrück Model and Periodic Boundary Conditions. *J. Phys. Chem. B* **2017**, *121* (15), 3443−3457.
(115) Vögele, M.; Köfinger, J.; Hummer, G. Hydrodynamics of Diffusion in Lipid Membrane Simulations. *Phys. Rev. Lett.* **2018**, *120* (26), 268104.
(116) Antila, H. S.; et al. Using Open Data to Rapidly Benchmark Biomolecular Simulations: Phospholipid Conformational Dynamics. *J. Chem. Inf. Model.* **2021**, *61* (2), 938−949.
(117) Filippov, A.; Orädd, G.; Lindblom, G. Effect of NaCl and CaCl(2) on the lateral diffusion of zwitterionic and anionic lipids in bilayers. *Chem. Phys. Lipids.* **2009**, *159* (2), 81−87.
(118) Filippov, A.; Orädd, G.; Lindblom, G. The effect of cholesterol on the lateral diffusion of phospholipids in oriented bilayers. *Biophys. J.* **2003**, *84* (5), 3079−3086.

https://doi.org/10.1021/acs.jcim.2c00395
J. Chem. Inf. Model. 2022, 62, 6462−6474